Coexisting structures from high- and low-energy precipitation in fine-scale aurora

H. Dahlgren,[1,2] B. S. Lanchester,[2] and N. Ivchenko[1]

Abstract. High resolution multi-monochromatic measurements of auroral emissions have revealed the first optical evidence of co-existing small-scale auroral features resulting from separate high and low energy populations of precipitating electrons on the same field line. The features exhibit completely separate motion and morphology. From emission ratios and ion chemistry modeling, the average energy and energy flux of the precipitation is estimated. The high energy precipitation is found to form large pulsating patches of 0.1 Hz with a 3 Hz modulation, and non-pulsating co-existing discrete auroral filaments. The low energy precipitation is observed simultaneously on the same field line as discrete filaments with no pulsation. The simultaneous structures do not interact, and they drift with different speeds in different directions. We suggest that the high and low energy electron populations are accelerated by separate mechanisms, at different distances from earth. The small scale structures could be caused by local instabilities above the ionosphere.

1. Introduction

Auroral displays contain a large amount of structuring with scale sizes perpendicular to the background magnetic field of orders of 100 m and less [e.g. Maggs and Davis, 1968; Trondsen and Cogger, 1998; Dahlgren et al., 2012]. The source of the structuring, and the acceleration mechanism of the precipitating electrons causing the fine scale aurora are not yet well understood [Sandahl et al., 2008]. Obliquely propagating inertial Alfvén waves interacting with cold electrons above the ionosphere are often thought to be related to the formation of the thinnest auroral forms [Stasiewicz et al., 2000; Semeter and Blixt, 2006]. However, Chaston et al. [2003] showed that Alfvén waves alone are unlikely to account for these auroral filaments.

Simulations and models have indicated that instabilities occurring on existing current sheets of precipitating electrons are a likely source for the structuring seen in the auroral emissions [e.g. Seyler, 1990; Otto and Birk, 1993; Chaston and Seki, 2010]. Transverse current gradients, shear flow and tearing due to electron inertia can give rise to instability growth in the region close to Earth which will cause striation of the current sheet and formation of fine scale structuring. To get a better understanding of the formation mechanism, the models need to be compared with measurements of the morphology, energy and energy flux of the resulting auroral features.

Electron data from the PHAZE II rocket showed a case of a so-called inverted-V structure with plasma sheet electrons accelerated to an energy of several keV, during which field-aligned bursts of cold electrons with a spread in energy from a few tens of eV up to the inverted-V energy, were seen superimposed [Semeter et al., 2001]. A similar event was observed with instruments on the Auroral Turbulence 2 rocket [Ivchenko et al., 1999], and the Cascades-2 rocket, where Alfvénic processes were found superimposed on a quasi-static acceleration signature [Mella et al., 2011; Lynch et al., 2012]. Time-dispersed field-aligned electron bursts by Alfvén waves have also been seen in an inverted-V structure with instruments on the Reimei satellite [Asamura et al., 2009], where the low energy populations were found to drive instabilities giving rise to vortical auroral forms. It was not possible in any of these studies to separate and correlate specific auroral forms with different electron populations.

In this paper we have estimated the energy of at least two precipitating populations of electrons, whose optical signatures are on the same field line simultaneously. The occurrence of such small scale auroral filaments, whose sources must be very different, is of importance for theoretical studies of the acceleration processes operating in the lower magnetosphere and above.

2. Instrumentation

ASK (Auroral Structure and Kinetics) is a ground-based optical instrument containing three highly sensitive identical imagers pointed at magnetic zenith. Each imager consists of an electron multiplying CCD (EMCCD), for which the 512 × 512 pixels are binned to 256 × 256 pixels, an F/1 lens system with a field-of-view (FOV) of 3.1° × 3.1°, and a narrow (FWHM ∼ 1 nm) interference filter. The first imager provides observations of emissions from the O_2^+ 1N band at 562.0 nm ($I_{O_2^+}$), which are caused by high energy precipitation penetrating down to the ionospheric E region. The second imager captures the forbidden O^+ emission at 732.0 nm (I_{O^+}), which has a lifetime of ∼5 s. This emission is produced in the F region due to low energy precipitation. At this wavelength there are also underlying N_2 emission bands, produced by high energy precipitation [Dahlgren et al., 2008a]. The third imager measures the atomic oxygen emission at 777.4 nm (I_O), which in the aurora is most sensitive to low energy precipitation [Lanchester et al., 2009] and results from direct excitation of atomic oxygen in the ionospheric F region. It is also produced by high energy precipitating electrons through dissociative excitation of molecular oxygen in the E region. The ratio of the two prompt emissions, $I_O/I_{O_2^+}$, can be used to estimate the average energy of the precipitation in the auroral features by comparing this ratio with modeled brightness ratios, which are calculated using a combined electron transport and ion chemistry model for different input energies at a specific energy

[1]Space and Plasma Physics, School of Electrical Engineering, Royal Institute of Technology, Stockholm, Sweden.

[2]Space Environment Physics, School of Physics and Astronomy, University of Southampton, Southampton, UK.

Copyright 2015 by the American Geophysical Union.
0148-0227/15/$9.00

flux [Lanchester and Gustavsson , 2012]. More information on ASK and the selected emissions is provided in Dahlgren et al. [2008b]. The ASK images are dark and flatfield corrected and background subtracted. The images are then smoothed using median and adaptive noise-removal filtering. The frame rate is 32 Hz and for this study 5 frames were averaged together to improve the signal-to-noise ratio. For the measurements discussed here, ASK was situated at the EISCAT site near Tromsø (19.2°E, 69.6°N). The EISCAT UHF radar was running the tau2pl experiment, making field-aligned measurements of the plasma parameters in the ionospheric E- and F-regions with a range resolution of 1.8 – 5.4 km.

3. Observations

The measurements were obtained during a large geomagnetic storm on the night of 14/15 December 2006, with many hours of highly disturbed geomagnetic conditions giving rise to extremely dynamic auroral displays. Thin, short-lived auroral filaments with narrow energy distributions around 8 keV have been reported from this night elsewhere [Dahlgren et al., 2012]. In the present study we examine the morphological differences observed between simultaneous and co-located emissions caused by high and low energy electrons in the early morning sector around 03:30 UT (∼06 MLT). In Figure 1, the top row of panels are overlaid snapshots from the three cameras color coded red, green and blue for $I_{O_2^+}$, I_{O+} and I_O, respectively, for 7 selected times within a 30 s interval, shown in the panels below. These panels are formed by stacking a time series of east-west slices taken through the center of the images. Panel 2 is the overlaid slices with the same color code as the snapshots, and the three lower panels are from each camera. The overlaid images and slices show clear morphological differences; emissions from high energy precipitation appear red-violet and are present throughout the interval, whereas completely separate auroral features due to low energy precipitation can be seen as green-blue slanting stripes (in panel 2) and as structured forms (in top row images 2 – 6).

The regular vertical stripes seen in the red-violet emissions in the overlaid slices indicate that the 'high energy aurora' is pulsating. Analysis of a longer time sequence of ASK data and data from a co-located allsky imager (data not shown here) indicate that these emissions come from Pc2 pulsating patches (0.1 - 0.2 Hz), with a faster brightness modulation of 3 Hz seen in the on-period. This 3 Hz modulation is particularly clear at around 03:38:24–29 UT. The pulsating patches have sharp boundaries (one such edge is evident from 03:38:13–18 UT and in the top row images 2 and 3). The pulsating emission occurs on top of other discrete high energy auroral filaments, e.g., the structure marked with a white arrow, corresponding to the narrow horizontal feature in images 4 and 5. Images 6 and 7 in the top row of Figure 1 show a pulsating patch switching from on at 03:38:34.0 UT to off 0.6 s later. A small non-pulsating auroral structure close to the center of the image remains as the pulsation switches off but has moved towards the southeast. No pulsations are seen in the 'low energy aurora'; the vertical stripes in the I_{O+} slices are due to the N_2 contamination in the same spectral region caused by the high energy precipitation.

The height distribution of the O_2^+ emission peaks at heights close to 100 km, whereas the O^+ emissions have a maximum at around 275 km, as drawn in Figure 2. Since the ASK imagers have the same FOV, the imager monitoring the O^+ emissions covers a larger horizontal area than the O_2^+ imager. A pixel-to-field-line transformation of the data is used, by which the O^+ images are mapped along the geomagnetic field lines to the same height as the O_2^+ images. This simple procedure allows a direct comparison of the features which are on the same field line, although occurring at very different heights.

Two examples of different structures are shown in Figure 3; these are the times marked a) and b) in Figure 1, which are 10 s apart. The gray scale images are I_{O+} and yellow contours from the co-existing features in the high energy channel, $I_{O_2^+}$, at levels of 180 R, 230 R and 280 R are overlaid. Below each combined image are the individual images from the three ASK cameras for the same time, with the location of magnetic zenith marked (+). Note that these images are rotated 90° in orientation from those in Figure 1. The full 30 s sequence is shown in the video in the auxiliary material, where pulsating auroral structures are seen in $I_{O_2^+}$ and I_O, drifting to the east. Several separate auroral fine scale structures appear in I_{O+} and move more slowly, towards north–northeast, often overlapping the structures in the other two channels. An analysis of the brightness of the O^+ emission shows that it is constant or increases with time in the structures (this can be seen in panels 2 and 4 in Figure 1), which is evidence that the auroral filaments are caused by continuous low energy electron precipitation and are not just the afterglow of the long-lived O^+ emission drifting with the plasma flow, which would decay with time.

At 03:38:16.156 UT (Figure 3a) an oval-shaped auroral feature (about 3 km × 9 km, at an assumed emission height of 275 km) is seen in I_{O+}. The feature is not present in the $I_{O_2^+}$ data, which indicates that it is solely the result of low energy precipitation with a stopping height in the F region. At the same time as the low energy feature moves across the I_{O+} image, a more intense auroral feature with a sharp edge moves in an eastward direction across the $I_{O_2^+}$ image. This intense feature can be seen in the $I_{O_2^+}$ image, and is outlined by the yellow contour in the overlaid image. The two emissions with different morphology and different drift speeds overlap as they move in slightly different directions. The direction of motion is marked in the bottom images with black arrows.

At 03:38:25.375 UT (Figure 3b) a very thin auroral filament stretches diagonally across the center of the I_{O+} image in the northwest-southeast direction, with no counterpart in the $I_{O_2^+}$ image. The full width at half maximum intensity of the filament is 210 m at an assumed emission altitude of 275 km. The structure drifts towards northeast, with a speed of 1.0 km/s. At the same time, faster moving (about 1.8 km/s) structures can be seen in the $I_{O_2^+}$ images; these structures drift in a predominantly eastward direction, and have widths of a few hundred meters. In Figure 3b, one of the high energy structures can be seen as a north–south aligned curved feature to the west in the $I_{O_2^+}$ image; it overlaps and crosses the low energy filament as it drifts to the east.

4. Energy estimation

The emission brightness ratios of $I_{O_2^+}$ and I_O can be used together with the combined electron transport [Lummerzheim and Lilensten, 1994] and ion chemistry model [Lanchester et al., 2001] to give an estimate of the average energy and energy flux of the precipitating electrons causing the emissions. Solar and geomagnetic conditions for the time and location are input to the model together with the neutral atmosphere from MSIS. The model gives estimates of production rates, from which are obtained integrated brightnesses for the ASK emissions, for a specified average energy and flux input. A more detailed description of the method and examples of model results can be found in Lanchester and Gustavsson [2012].

The energy of the structured pulsations was analysed using this method. The temporal variation of the emission ratio was investigated for a small region centered on magnetic zenith. The ratio analysis presented in Figure 4a is for the time 03:38:14.5 UT, which is marked with an asterisk in Figure 1. It corresponds to the time that the O_2^+ patch, seen 2 s later in Figure 3a, passes through the magnetic zenith. The scatter plot is I_{O^+} against $I_{O_2^+}$ for all pixels within the region marked in Figure 4b. A linear fit to the data, forced to pass through the origin, shows that the average energy in the area of the box is 28 ± 5.0 keV. The energy flux can also be estimated from the ion chemistry model and the $I_{O_2^+}$ brightness. For energies above 1 keV the modeled relation between brightness and flux is approximately 10 R/mWm^{-2}, so that the measured average $I_{O_2^+}$ brightness of 180 R within the box corresponds to an energy flux of approximately 18 mWm^{-2}. Precipitating electrons with an energy of close to 30 keV penetrate to below 100 km in the ionosphere [Rees, 1989]. Electron density as a function of time and height provided by the EISCAT UHF radar at 10 s resolution is shown in Figure 4c. The time when the bright, energetic ($I_{O_2^+}$) aurora passed the radar beam is marked with an arrow in Figure 4c and the corresponding density profile is shown in Figure 4d. These data support the finding of energetic electron precipitation of at least 30 keV, with an ionization peak well below 100 km altitude at the time of the pulsating auroral structures.

The same emission ratio method cannot be used to estimate the energy of the low energy structures seen in I_{O^+}, since there is no detectable emission above the noise level in $I_{O_2^+}$. However, results from the ion chemistry model demonstrate that the production of excited O^+ ions is most sensitive to precipitation of low energy electrons of about 200 eV, which results in an emission peak above 250 km.

5. Discussion and Conclusions

The unique imaging capabilities of the ASK instrument mean that it is possible to separate auroral emissions caused by precipitation of different characteristics at very high temporal and spatial resolution. The data presented here demonstrate that two different, decoupled source populations can co-exist and the accelerated electrons reach the same region in the ionosphere, giving rise to overlapping auroral emissions with different spectral and morphological characteristics. During a prolonged interval of high energy precipitation, which exhibits structured features and pulsations, there also appear low energy features that exhibit no pulsations, with completely different morphology and motions. Both the high and low energy aurora are highly structured, with sharp edges and narrow widths, and cross and overlap as they move across the ASK FOV.

To compare the auroral filaments occurring at different heights, the $I_{O_2^+}$ image was scaled according to the height difference and overlaid on the I_{O^+} image with the location of magnetic zenith aligned. While the mapping could be improved by using a geomagnetic field model, a direct scaling is sufficient for the small FOV of ASK with the aurora occurring close to or in magnetic zenith, as is the case for the overlapping structures investigated here. The assumption that the auroral emissions originate from a single altitude layer is a simplification, but does not affect the result.

Pulsations in energetic electron precipitation are believed to be driven by wave-particle interactions, such as whistler wave modes near the geomagnetic equator [e.g. Nishimura et al., 2011, and references therein]. The 3 Hz modulation of pulsations have been observed previously by rockets [e.g. Sandahl et al., 1980] and in a few ground-based observations [Samara and Michell, 2010; Nishiyama et al., 2014] but their generation mechanism remains unexplained. The observations presented here of high energy Pc2 pulsations with 3 Hz modulations on top of non-pulsating auroral structures also indicate multiple processes occurring simultaneously.

The low energy precipitation is likely to be generated by acceleration of cold electrons just above the ionosphere by the parallel electric field component of obliquely propagating Alfvén waves. The motion of optical structures directly resulting from the precipitation would then be governed by the motion of the source waves.

The narrow structures seen in the emissions from high energy precipitation, which are non-pulsating, are typical of small scale filamentary aurora, which have been described theoretically by Otto and Birk [1993], and demonstrated in e.g. Lanchester et al. [1997]. In this plasma-neutral simulation the filamentation occurs through instabilities close to the ionosphere, at about 1 – 2 R_E, altering the magnetic topology. Further inspection of ASK data sets should shed light on whether co-existing low and high energy aurora is a common phenomenon. The properties of the auroral features, such as energy of precipitation, changes in brightness, velocity of optical features and their small scale morphology should be used as input to such simulations in order to understand the origin of the different populations causing the auroral variations.

Acknowledgments. This work was supported by the Swedish Research Council under grant 350-2012-6591. EISCAT is an international association supported by research organizations in China (CRIRP), Finland (SA), France (CNRS, until end 2006), Germany (DFG), Japan (NIPR and STEL), Norway (NFR), Sweden (VR), and the United Kingdom (STFC and NERC). We thank Mike Kosch for providing all-sky camera data to help give context to the ASK observations, and Sam Tuttle for valuable suggestions during the completion of this research. Requests for data used in this paper can be directed to Hanna Dahlgren (hannad@kth.se).

References

Asamura, K., C. C. Chaston, Y. Itoh, M. Fujimoto, T. Sakanoi, Y. Ebihara, A. Yamazaki, M. Hirahara, K. Seki, Y. Kasaba, and M. Okada (2009), Sheared flows and small-scale Alfvén wave generation in the auroral acceleration region, *Geophys. Res. Lett., 36*, L05105, doi:10.1029/2008GL036803.

Chaston, C. C., Peticolas, L. M., Bonnell, J. W., Carlson, C. W., Ergun, R. E., McFadden, J. P., and Strangeway, R. J. (2003), Width and brightness of auroral arcs driven by inertial Alfvén waves, *J. Geophys. Res., 108*,SIA 17-1.

Chaston, C. C., and K. Seki (2010), Small–scale auroral current sheet structuring, *J. Geophys. Res., 115*, A11221, doi: 10.1029/2010JA015536.

Dahlgren, H., N. Ivchenko, B. Lanchester, J. Sullivan, D. Whiter, G. Marklund, and A. Stromme (2008a), Using spectral characteristics to interpret auroral imaging in the 731.9 nm O^+ line, *Ann. Geophys., 26*, 10951917, doi:10.5194/angeo-26-1041-2008.

Dahlgren, H., N. Ivchenko, J. Sullivan, B. S. Lanchester, G. Marklund, and D. Whiter (2008b), Morphology and dynamics of aurora at fine scale: first results from the ASK instrument, *Ann. Geophys., 26*, 10411048, doi:10.5194/angeo-26-1041-2008.

Dahlgren, H., N. Ivchenko, and B. S. Lanchester (2012), Monoenergetic high-energy electron precipitation in thin auroral filaments, *Geophys. Res. Lett., 39*, L20101, doi: 10.1029/2012GL053466.

Ivchenko, N., G. Marklund, K. Lynch, D. Pietrowski, R. Torbert, F. Primdahl, and A. Ranta (1999), Quasiperiodic oscillations observed at the edge of an auroral arc by Auroral Turbulence 2, *Geophys. Res. Lett., 26*, 33653368, doi:10.1029/1999GL003588.

Lanchester, B. S., M. H. Rees, D. Lummerzheim, A. Otto, H. U. Frey and K. U. Kaila (1997), Large fluxes of auroral electrons in filaments of 100 m width, *Geophys. Res. Lett., 102*, 9741–9748.

Lanchester, B. S., M. H. Rees, D. Lummerzheim, A. Otto, K. J. F. Sedgemore-Schulthess, H. Zhu, and I. W. McCrea (2001), Ohmic heating as evidence for strong field-aligned currents in filamentary aurora, *J. Geophys. Res., 106*, 1785–1794.

Lanchester, B. S., M. Ashrafi, N. Ivchenko (2009), Simultaneous imaging of aurora on small scale in OI (777.4 nm) and N21P to estimate energy and flux of precipitation, *Ann. Geophys., 27*, 2881–2891.

Lanchester, B. S. and B. Gustavsson (2012), Imaging of aurora to estimate the energy and flux of electron precipitation, Auroral Phenomenology and Magnetospheric Processes: Earth and Other Planets (eds A. Keiling, E. Donovan, F. Bagenal and T. Karlsson), American Geophysical Union, Washington, D. C., doi:10.1029/2011GM001161.

Lummerzheim, D. and J. Lilensten (1994), Electron transport and energy degradation in the ionosphere: Evaluation of the numerical solution, comparison with laboratory experiments and auroral observations, *Ann. Geophys., 12*, 1039–1051.

Lynch, K. A., D. Hampton, M. Mella, B. Zhang, H. Dahlgren, M. Disbrow, P. M. Kintner, E. Lundberg, and H. C. Stenbaek-Nielsen (2012), Structure and dynamics of the nightside poleward boundary (1): sounding rocket and groundbased observations of auroral electron precipitation in a rayed curtain, *J. Geophys. Res., 117*,A11202, doi:10.1029/2012JA017691.

Maggs, J. E. and T. N. Davis (1968), Measurements of the thicknesses of auroral structures, *Planet. Space Sci., 16*, 205–209.

Mella, M. R., K. A. Lynch, D. L. Hampton, H. Dahlgren, P. M. Kintner, M. Lessard, D. Lummerzheim, E. T. Lundberg, M. J. Nicolls, and H. C. Stenbaek-Nielsen (2011), Sounding rocket study of two sequential auroral poleward boundary intensifications, *J. Geophys. Res., 116*, A00K18, doi: 10.1029/2011JA016428.

Nishimura, Y., J. Bortnik, W. Li, R. M. Thorne, L. Chen, L. R. Lyons, V. Angelopoulos, S. B. Mende, J. Bonnell, O. Le Contel, C. Cully, R. Ergun, and U. Auster (2011), Multievent study of the correlation between pulsating aurora and whistler mode chorus emissions, *J. Geophys. Res., 116*, A11221, doi: 10.1029/2011JA016876.

Nishiyama, T., T. Sakanoi, Y. Miyoshi, D. L. Hampton, Y. Katoh, R. Kataoka, and S. Okano (2014), Multiscale temporal variations of pulsating auroras: On-off pulsation and a few Hz modulation, *J. Geophys. Res., 119* 35143527, doi:10.1002/2014JA019818.

Otto, A. and G. T. Birk (1993), Formation of thin auroral arcs by current striation, *Geophys. Res. Lett., 20*,2833-2836.

M. H. Rees (1989), Physics and chemistry of the upper atmosphere. Cambridge University Press, Cambridge, Great Britain.

Samara, M., and R. G. Michell (2010), Ground–based observations of diffuse auroral frequencies in the context of mode chorus, *J. Geophys. Res., 115*, A00F18, doi:10.1029/2009JA014852.

Sandahl, I., L. Eliasson, and R. Lundin (1980), Rocket observations of precipitating electrons over a pulsating aurora, *Geophys. Res. Lett., 7*, 309–312.

Sandahl, I., T. Sergienko, and U. Brändström (2008), Fine structure of optical aurora, *J. Atmos. Solar-Terr. Phys., 70*, 2275–2292.

Semeter, J., J. Vogt, and G. Haerendel: Persistent quasiperiodic precipitation of suprathermal ambient electrons in decaying auroral arcs, J. Geophys. Res., 106, 12 863–12 873, doi: 10.1029/2000JA000136.

Semeter, J. and E. M. Blixt (2006), Evidence for Alfvén wave dispersion identified in high-resolution auroral imagery, *Geophys. Res. Lett., 33*,L13106, doi:10.1029/2006GL026274.

Seyler, C. E. (1990), A mathematical model of the structure and evolution of small-scale discrete auroral arcs, *J. Geophys. Res., 95*, 95, 17,199.

Stasiewicz, K., P. Bellan, C. Chaston, C. Kletzing, R. Lysak, J. Maggs, O. Pokhotelov, C. Seyler, P. Shukla, L. Stenflo, A. Streltsov, and J.-E. Wahlund (2000), Small scale Alfvénic structure in the aurora, *Space Science Reviews, 92*, 423–533.

Trondsen, T. S., and L. L. Cogger (1998), A survey of small-scale spatially periodic distortions of auroral forms, *J. Geophys. Res., 103*, 9405 9416.

Corresponding author: H. Dahlgren, Space Environment Physics Group, School of Physics and Astronomy, University of Southampton, Southampton, SO17 1BJ, United Kingdom. (hannad@kth.se)

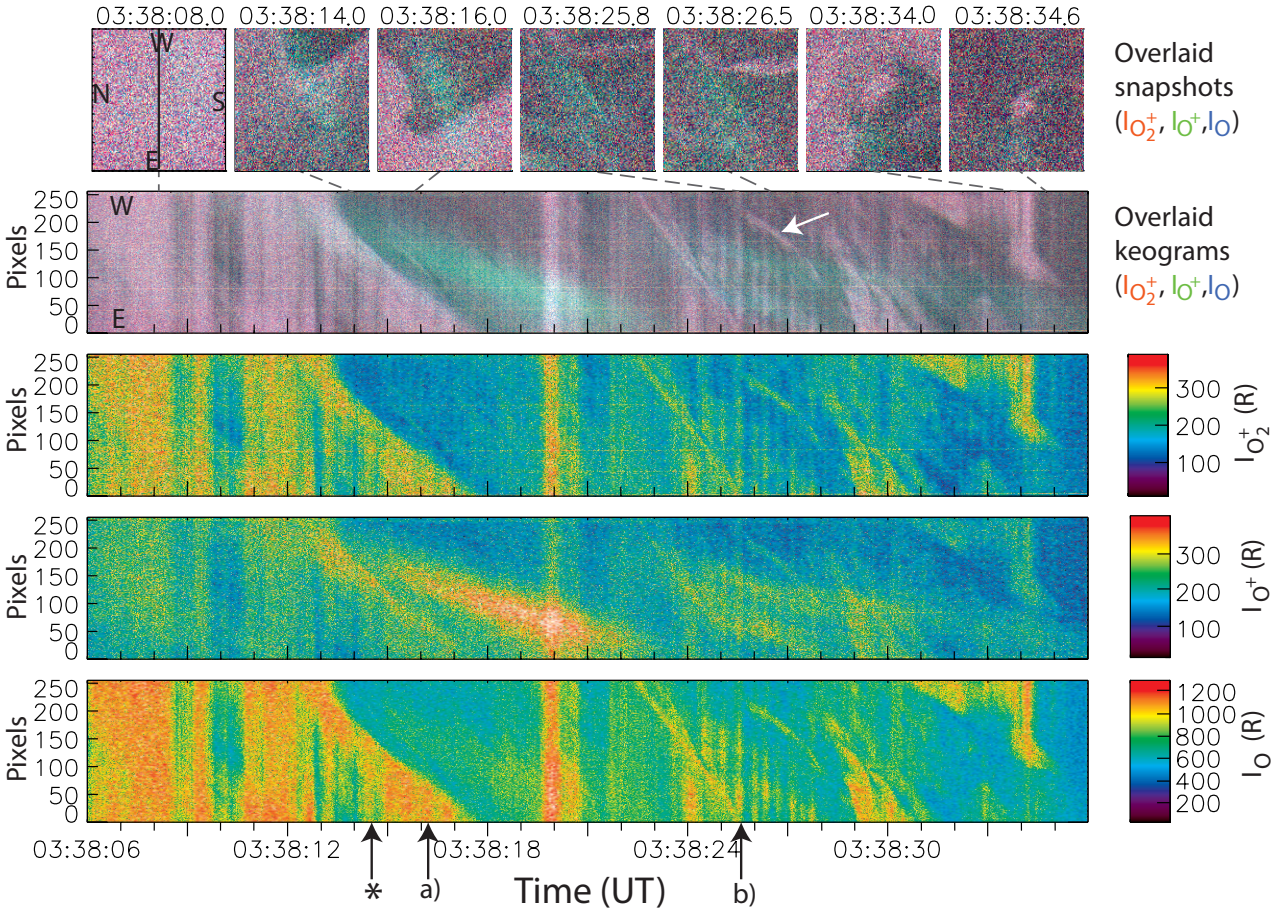

Figure 1. Top row: Snapshots of overlaid ASK images, color-coded $I_{O_2^+}$ (red), I_{O^+} (green) and I_O (blue). The cardinal directions are marked in the first image, together with a line marking the position of the slice used in the time series of slices below. Bottom 4 panels: 30 s interval, with top panel being the color-coded overlaid slices, followed by $I_{O_2^+}$, I_{O^+} and I_O. The black arrows marked *, a) and b) indicate the times of the data discussed in Figures 3 and 4.

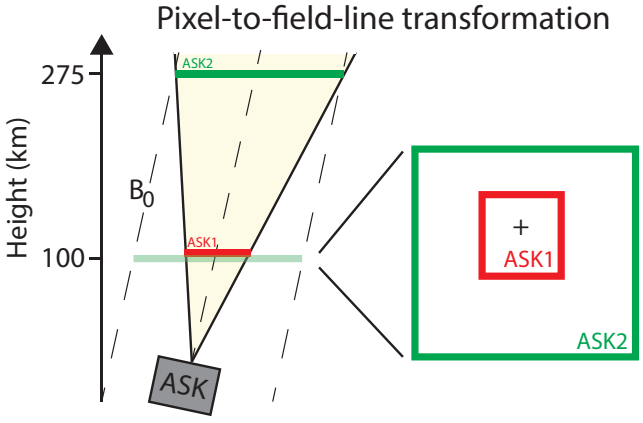

Figure 2. To compare the auroral morphology of the O^+ emissions in the F region with the O_2^+ emissions in the E region, the ASK2 image is mapped along the geomagnetic field lines down to 100 km, resulting in the overlaid ASK1 ($I_{O_2^+}$) and ASK2 (I_{O^+}) images of different size shown to the right. Magnetic zenith (marked with a black +) is in the same location in both images.

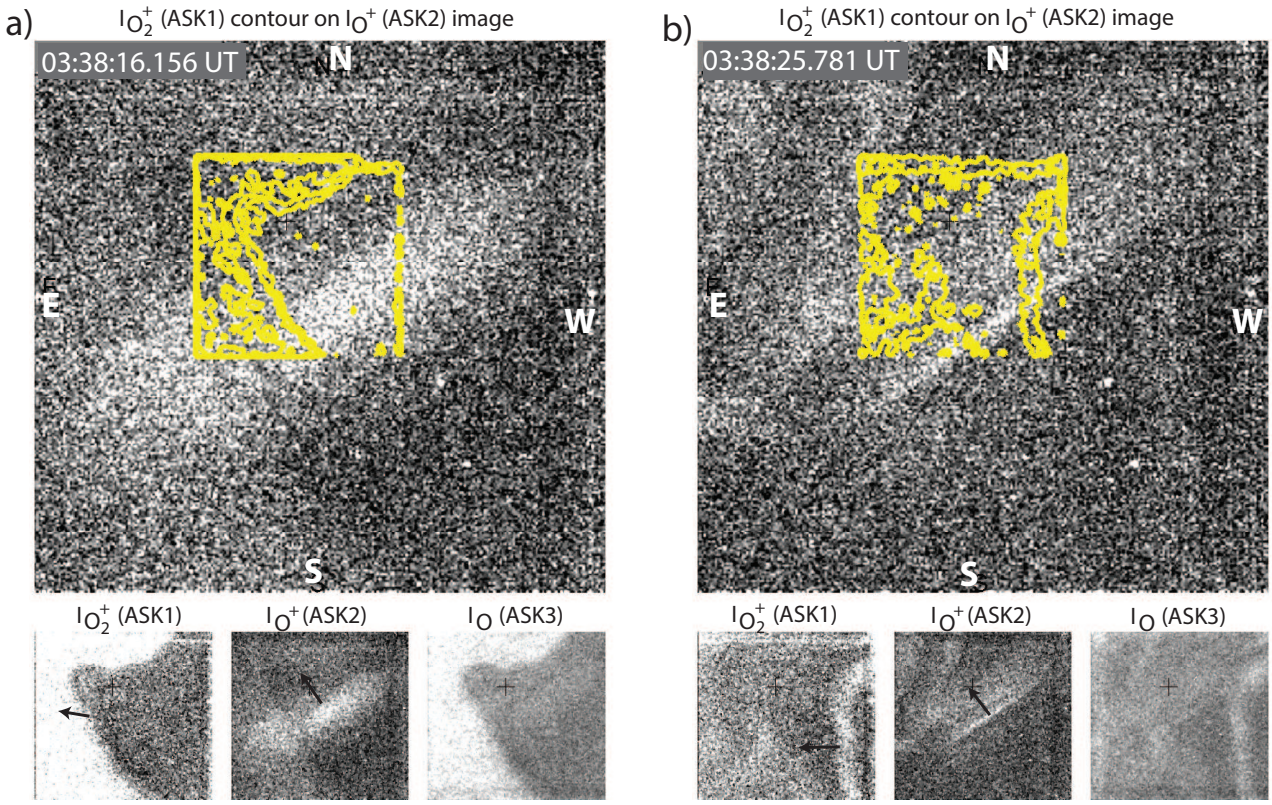

Figure 3. (a) Top panel: ASK I_{O^+} image (gray scale) mapped to 100 km altitude, with ASK $I_{O_2^+}$ image overlaid as contours, at 03:38:16.156 UT. North is up and east to the left in each image. Bottom panels: the individual snapshots from the three ASK cameras, with magnetic zenith marked as a +. The different morphology is evident in $I_{O_2^+}$ and I_{O^+}, and both high and low energy structures can be seen in the third imager (I_O). The direction of motion of the discussed structures are shown with black arrows. (b) Same setup as in (a) at 03:38:25.781 UT with a very narrow structure in I_{O^+} and a wider curved structure in $I_{O_2^+}$.

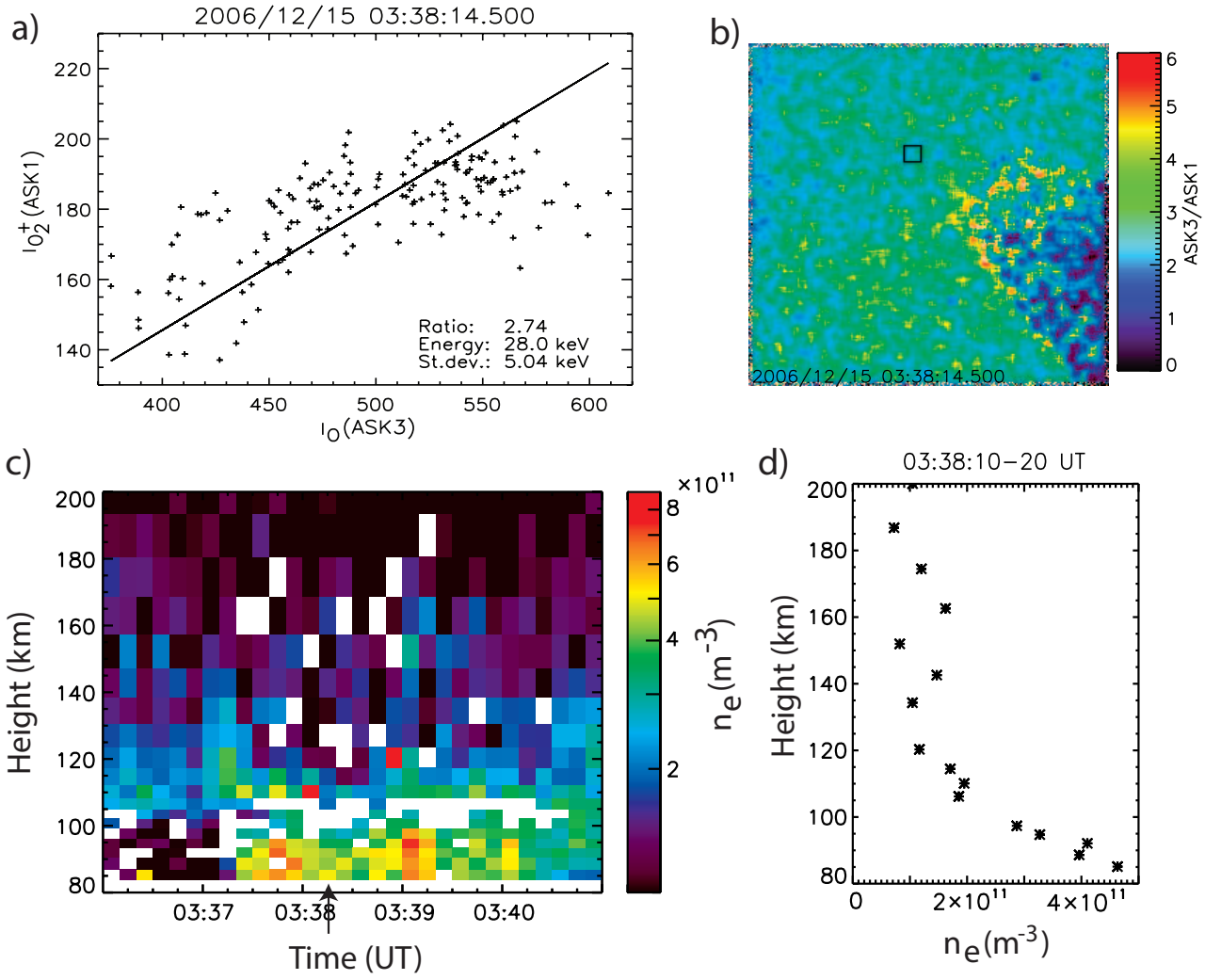

Figure 4. (a) I_O vs. $I_{O_2^+}$ per pixel in an area close to magnetic zenith in the ASK images, at 03:38:14.5 UT. This area is marked as a black square in the ratio image shown in (b). A linear fit to the data points give a ratio of 2.7, which corresponds to an energy of the precipitating electrons of about 28 keV. (c) Electron density vs. height and time from the EISCAT UHF radar shows an ionization peak below 80 km at the time of the optical observations. (d) The electron density profile at the time marked with an arrow in c), corresponding to the time of the ASK data shown in a) and b).